The Magnetization Mechanism in Single-Crystal Garnet Slabs Near the Compensation Temperature

Abstract: The magnetization mechanism has been studied in detail in single-crystal slabs of (111), (110) and (100) samples of gadolinium iron garnet (GdIG) near the compensation temperature. Using Faraday-effect and induction-type hysteresigraphs, the hysteresis loops have been measured in the sample plane and perpendicular to it, respectively. Measurements have been made at various temperatures, thus allowing the effects of variation of the saturation magnetization to be studied. In this way different relative magnitudes of shape and crystal anisotropy are obtained. Also, the effects of strain anisotropy variation are studied on the (111) sample. The hysteresis loops are correlated with the observed domain structures and a satisfactory theoretical model is described. Based on these studies, it is possible to estimate the approximate domain wall thickness and energy in GdIG. Finally, an estimate of the exchange constant is made which is comparable with other estimates.

Introduction

Application of ferrimagnetic garnet plates in beam addressable memories has been proposed and discussed recently by Chang, Mee, and others. They describe the use of a thermomagnetic writing process which relies on the rapid reduction of coercive force for small temperature changes in the region of the compensation temperature.

In this paper, the magnetization mechanisms in thin single-crystal garnet slabs are studied by Faraday-effect and induction-type hysteresigraphs and by domain observations using the Faraday effect. Since the slabs are transparent, the Faraday effect may be used to study the magnetization mechanism for applied fields perpendicular to the plates. At the same time the magnetization, although small, can be detected in the plane of the plates by a conventional induction method. Hence, a unique opportunity is afforded to study the hysteresis loops of a material in two directions and to correlate them with the domain structure. Moreover, the saturation magnetization may be controlled by varying the temperature.

Saturation magnetization, in the work to be described, varies between $M_{\rm s}=0$ and $M_{\rm s}\approx20$ gauss. This allows for the relative magnitudes of shape, crystal and strain anisotropics to be changed, and the corresponding effects on the magnetization mechanism to be studied.

The sections that follow cover in detail the magnetization mechanism for a (111) gadolinium iron garnet slab, with a dominant uniaxial stress anisotropy. Also described is a satisfactory theoretical model. From this study, it is possible to estimate the uniaxial anisotropy, the wall energy and the

wall thickness. In addition, an estimate of the exchange constant for GdIG can then be made. Finally, the effects of removing the stress anisotropy are measured. Both (110) and (100) plane samples are similarly examined and their magnetization mechanisms deduced.

Experimental procedures

Thin sections $(40-100\mu)$ of single crystals were prepared by cutting and polishing specimens from bulk single crystals. Rough cutting was performed with a diamond saw and polishing followed through a number of grades, ending with 0.3μ alumina powder. This polishing process introduced a uniaxial compressive strain perpendicular to the plane of the plates. Subsequently, the strain was annealed out by heating in air to 1100° C for one hour, followed by slow cooling.

Observations of the domain structure using the Faraday effect followed the techniques described by Dillon.³

The 60-Hz magnetic hysteresis loops were measured with the equipment shown schematically in Fig. 1. Here the garnet slab C is held in thermal contact with a thermoelectric element capable of controlling temperature within 0.5 °C between -20 °C and +80 °C. (Details of the hysteresigraph design will be given in a separate publication. 4) The electromagnet A is capable of applying a maximum field of 2,500 Oe perpendicular to the plane of the slab. A polarized He–Ne laser beam (about 1 mm in diameter), which serves as the detection light beam, passes through the sample to a detector. The detector is a differential type similar to that

468

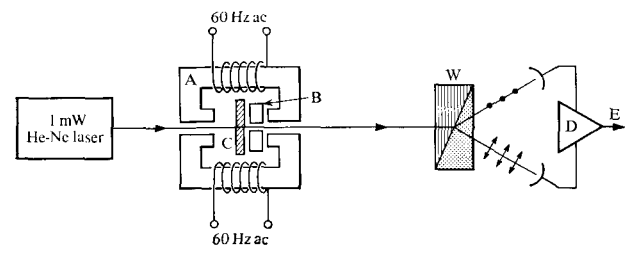


Figure 1 Faraday-effect 60 cps hysteresigraph. A—Magnetizing yoke. B—Thermoelectric element. C—Garnet sample. W—Wollaston prism, D—Differential amplifier.

described by Miyata⁵ in which the Faraday-rotated beam is polarized at 45° to the axes of a Wollaston prism. Two beams of 90° relative polarization direction are produced as shown in Fig. 1. These beams are directed onto silicon diode detectors from which electrical outputs are subtracted, giving zero output at E. If the polarization of the beam incident on the Wollaston prism rotates from the 45° position, the intensities of the beams on the solar cells are different, and an output is obtained at E. In this way, the signal at E is a 60-Hz depiction of the Faraday rotation of the sample. On reversing the magnetization M_s , the change in the intensities on the two detectors is $\pm I_1 \sin 2\phi$ ($I_1 =$ intensity transmitted by garnet sample). Hence, for small rotations, the output signal is proportional to the Faraday rotation ϕ . This signal is fed to the y plates, and a signal proportional to the sinusoidal field is fed from the electromagnet to the x plates of a cathode ray tube to show the Faraday-effect hysteresis loop. Due to the use of the differential detector, the equipment may be operated in normal room lighting and is not sensitive to much of the amplitude modulation in the laser source.

The measurement of the 60-Hz induction hysteresis loops in the plane of the garnet films was achieved by using a conventional hysteresigraph.⁶

Domain structures and magnetization curves

• Single-crystal slab (111)

All of the single-crystal slabs were of the order of 0.5×0.5 cm and were about 50μ thick. The GdIG sample was carefully mechanically polished, which induced a uniaxial stress anisotropy perpendicular to the plane of the slab.³ As will be seen, this stress anisotropy is significant with respect to the rather small crystal anisotropy and plays a major role in determining the magnetization properties. The M-H loops near the compensation temperature, measured with the Faraday-effect hysteresigraph, are shown in Fig. 2 for this as-polished sample. All of the loops correspond to the temperature range $+30\,^{\circ}$ C to $-5.8\,^{\circ}$ C with a compensation temperature at $+9.6\,^{\circ}$ C. Except for temperatures very near

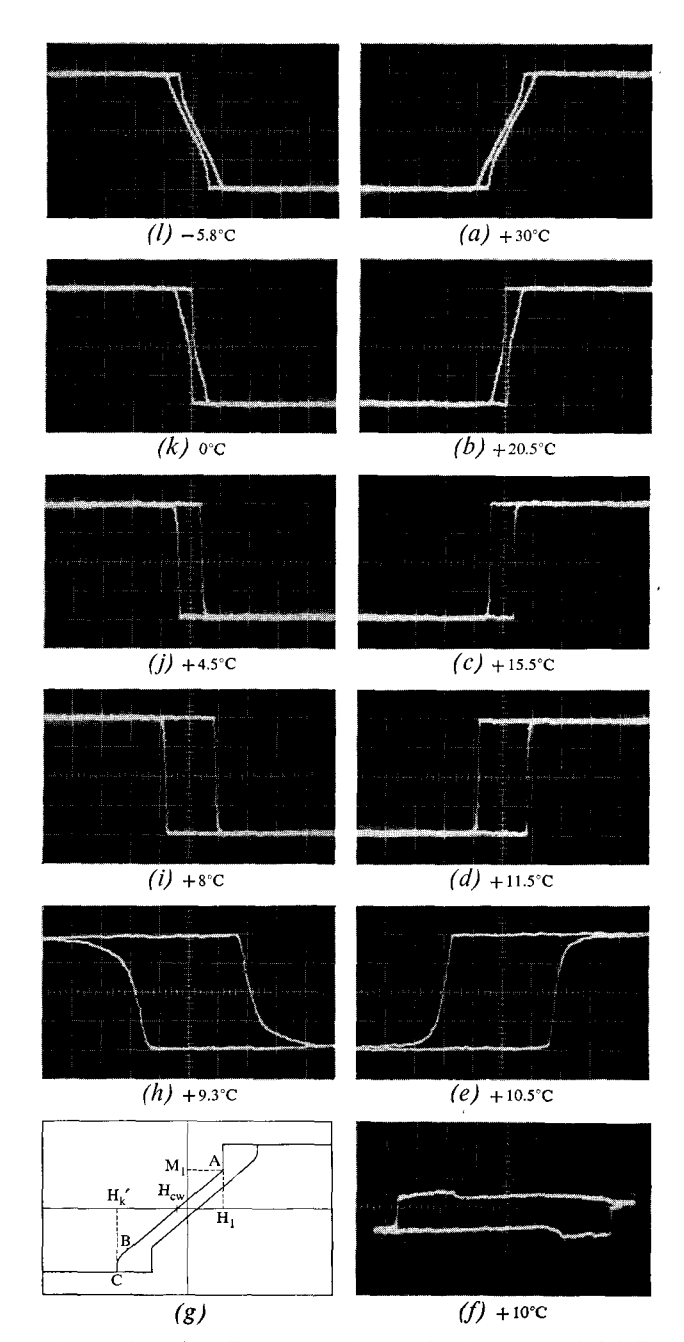
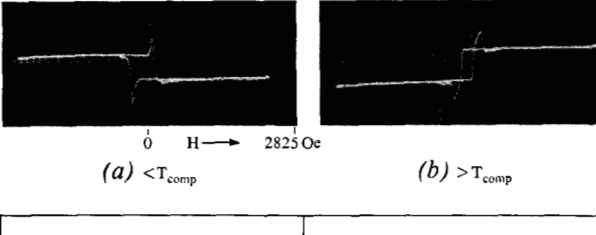


Figure 2 Faraday-effect hysteresis loop for single-crystal GdIG (111). H = 74 Oe/div.

to the compensation temperature $T_{\rm comp}$, the loop height is constant even though $M_{\rm s}$ changes rapidly with temperature; however, the loops are reversed for temperatures below $T_{\rm comp}$. Both of these effects result from the fact that the Faraday rotation is due to iron ions. Magnetization of the iron component is reasonably constant in the vicinity of $T_{\rm comp}$, and its direction, with respect to the applied field, is reversed as the temperature passes through $T_{\rm comp}$. Hence, provided the applied field is sufficient to saturate the



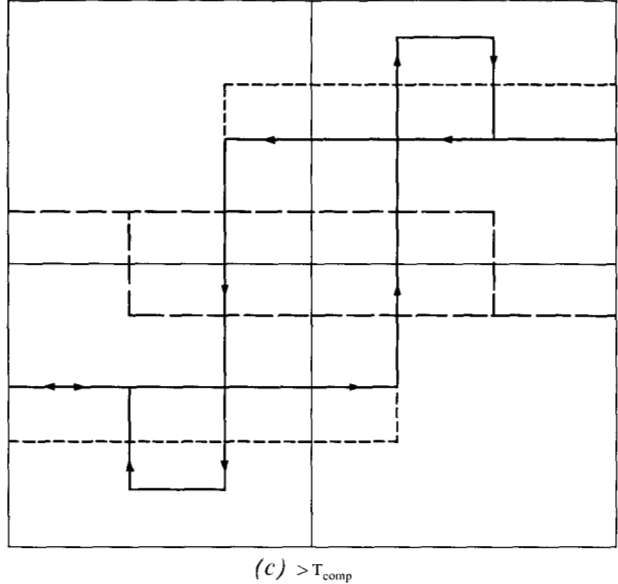


Figure 3 (a) and (b) Hysteresis loop distortion near $T_{\rm comp}$. H=56.5 Oe/div. (c) Schematic representation of Figure 2(b) (solid loop) as the addition of two component loops (dotted).

sample, constant rotation is obtained. The reduction in loop height (Fig. 2f) near T_{comp} occurs because there is increased coercive force near T_{comp} and a minor hysteresis loop is obtained. The bumps occurring on this M-H loop are an anomalous effect caused either by a temperature gradient in the field of view of the laser beam, or by a variation of compensation temperature of the material within the field of view. An exaggerated case of this type of loop distortion is demonstrated in Fig. 3 (a and b) in which a temperature gradient is deliberately introduced near T_{comp} . The result is reduced loop height, the appearance of anomalous peaks, and a change in coercive force. These loops are, in fact, the summation of loops from material which is above and below T_{comp} . This effect is demonstrated in a simple way in Fig. 3(c) with two component loops (dotted) leading to the resultant solid line loop.

The set of hysteresis loops in Fig. 2 can be divided into three groups. For temperatures more than $\pm 10^{\circ}$ C from T_{comp} [Fig. 2 (a,b,k,l)], the nucleation of the first reversal from saturation occurs for a reverse applied field which is less negative than the wall coercive force H_{cw} , as is drawn at point A in Fig. 2(g). At this applied field H_1 , the first reverse domain occurs near an inhomogeneity [e.g., scratch shown in the domain pattern of Fig. 4(b)] where local

stresses reduce the nucleation field required to form a reversed domain. This nucleation field H_n is given approximately by

$$H_{\rm n} = 4\pi M_{\rm s} - H_{\rm 1}, \tag{1}$$

where $4\pi M_s$ is the demagnetization field.

Rapid magnetization reversal occurs at H_1 , and thus the demagnetizing field NM_s reduces rapidly until the total reverse field falls below that required to propagate domain wall motion; this field is the domain wall coercive force, H_{cw} . Hence, if M_1 is the magnetization reached in this reversal (Fig. 2g)

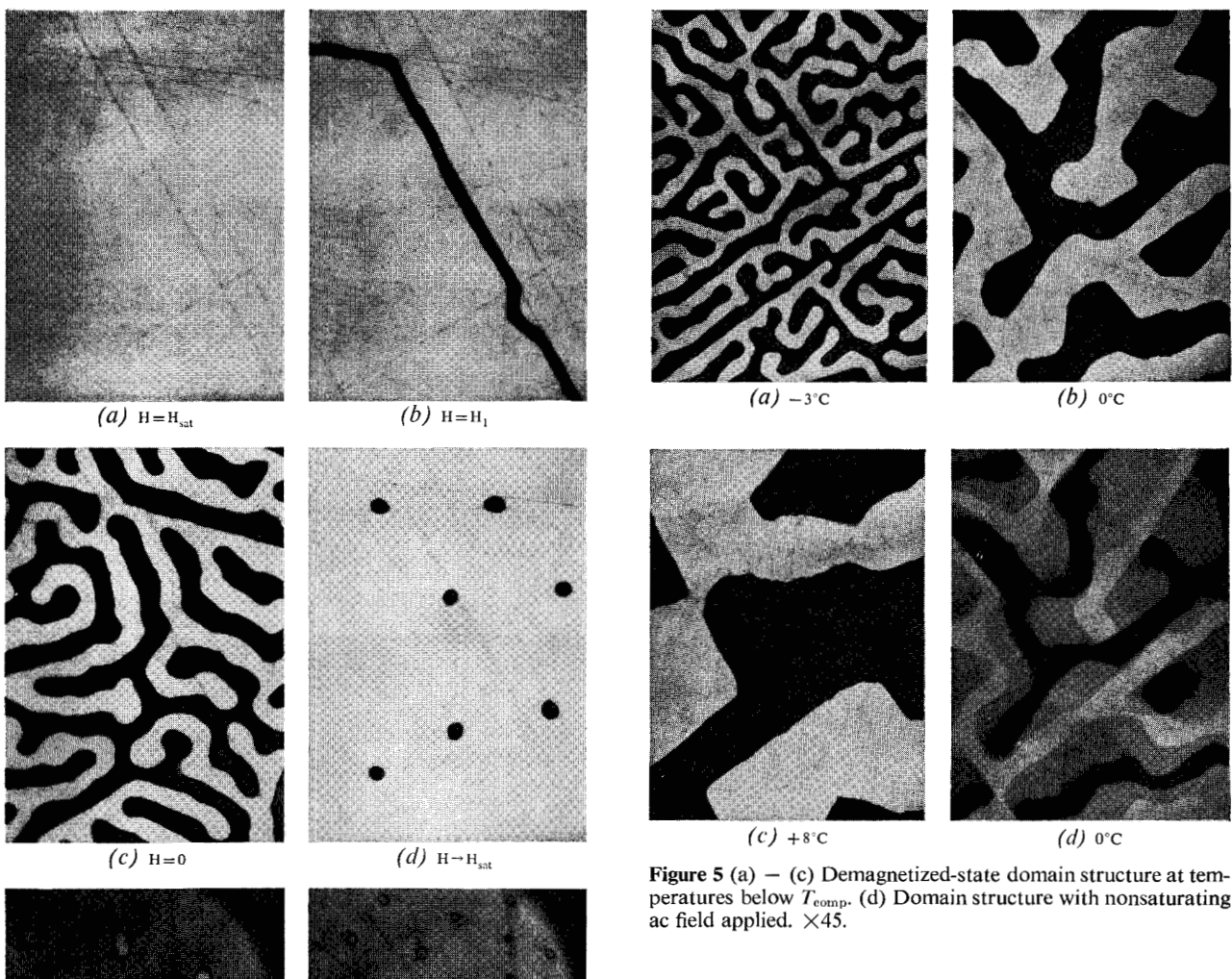
$$H_{\rm ew} = NM_1 - H_1, \tag{2}$$

where N is the demagnetizing factor.

On further reducing the applied field, the reduction of M is controlled by the corresponding reduction of NM until the resultant field falls to $H_{\rm cw}$. This mechanism accounts for the constant-slope portion of the loop from A to B [Fig. 2(g)]. The reverse domains continue to increase in number and area in this region and the structure in Fig. 4(c) is obtained as the applied field reduces to zero. As negative saturation is approached, in region C, the slope of the M-H curve again increases and saturation is reached at a field $H_k' < 4\pi M_s$. At this stage, the remaining unreversed domains decrease in length to produce small circular domains [Fig. 4(d)] of approximately constant diameter. The magnetization behavior is amenable to more detailed analysis and is discussed further in the last section of this paper.

For temperatures close to $T_{\rm comp}$, $M_{\rm s}$ is reduced and a relatively larger magnetization reversal occurs at nucleation as shown in Fig. 2 [(b) and (k)]. Furthermore, for an applied field approaching $H_{\rm sat}$, the circular domains are larger in diameter and fewer in number [Fig. 4(e)] at $T=17\,^{\circ}\mathrm{C}$ (compared with Fig. 4(f) at $T=32\,^{\circ}\mathrm{C}$). There appears to be less interaction between these domains and the surface scratches at these temperatures than at higher temperatures. Thus, the barriers to domain wall motion increase with increasing $M_{\rm s}$. However, this does not necessarily lead to an increase of the measured coercive force, since the torque in the magnetization, and hence the force applied to move the wall, will increase with increasing $M_{\rm s}$.

In the second group of M-H loops, Fig. 2(c,d,i,j), the reverse field required for nucleation exceeds the saturation field H_k and complete magnetization reversal occurs. At temperatures within about 1° of $T_{\rm comp}$, [Fig. 2(e,h)] the saturation field exceeds $H_{\rm n}$, resulting in nonsquare loops. This is probably due to temperature and compensation-point variations within the field of view. Even closer to the compensation temperature, the applied field is sufficient only to partially switch the material, and a minor loop of irregular shape occurs as shown in Fig. 2(f). Another cause of the irregular loop shapes is that the domain size increases



peratures below $T_{\text{comp.}}$ (d) Domain structure with nonsaturating

Figure 4 Domain structure on GdIG (111) single crystal. (a) to (d), T = 25°C; (e) T = 17°C; (f) T = 32°C. $\times 100$.

(f) $T=32^{\circ}C H \rightarrow H_{sat}$

(e) $T=17^{\circ}C H \rightarrow H_{sat}$

rapidly as T_{comp} is approached. This is shown by the a-c demagnetized domain patterns in Fig. 5(a-d). Within a few degrees of T_{comp} the domain size approaches that of the laser beam, and the average magnetization of the sample is no longer detected. The observed loops then vary as a function of position on the sample. Fig. 5(d) shows the 0°C domain structure with an a-c field applied ($H_{ac} = 0.5 H_{s}$). Here the effect of the surface scratches on pinning the domain boundaries is clearly seen. The scratches appear to be the most effective inhomogeneities impeding domain wall motion.

Magnetization loops have also been measured on this same sample in the sample plane using an induction-type 60 Hz M-H loop plotter. Here, the loop height diminishes as T_{comp} is approached since the total magnetization is measured. Typical loops are shown in Fig. 6(a-d), and no change was found for different in-plane directions. These loops have essentially no hysteresis, and a rotational magnetization process is assumed. This is supported by the evidence of rotation in the domain structure when a field is applied in the plane [Fig. 7(b)]. That the initial magnetization mechanism is a rotational one can be seen from the corresponding domain structures in Fig. 7(a,b). In Fig. 7(a), the magnetization lies in the plane of the sample only at the domain boundaries and these are revealed as black lines. On applying a horizontal field [Fig. 7(b)], shaded zones appear near the surface scratches, indicating rotation of the magnetization towards the sample plane. For the room-temperature hysteresis loop of Fig. 6(a), there is a change of slope in the region of H = 140 Oe. At this field, all of the original domains disappear and the magnetization mode changes.

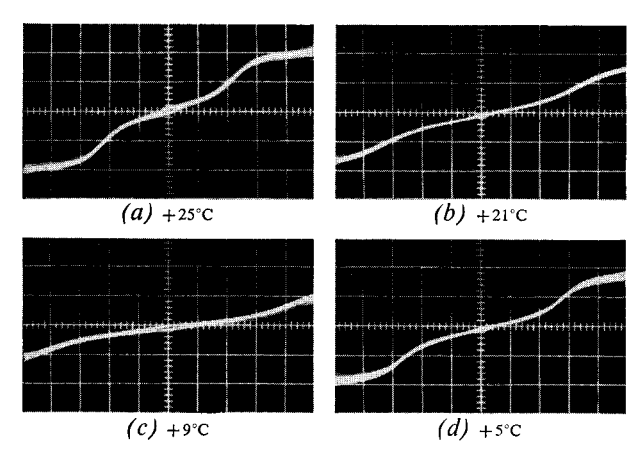
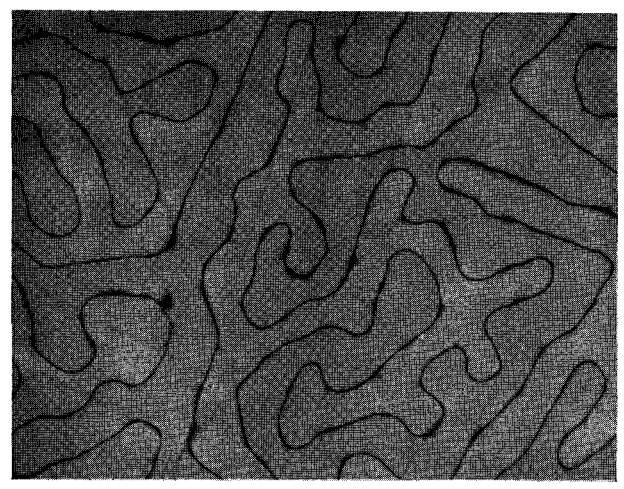
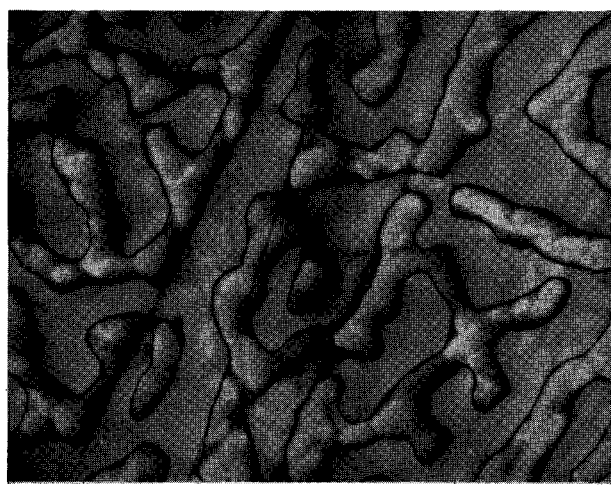


Figure 6 In-plane inductive M-H loops on GdIG (111). $H_{\text{max}} = 580$ Oe.

Figure 7 Effect of in-plane field on GdIG (111) domain structure. The analyzer was adjusted to reveal domain boundaries. $T = 28^{\circ}\text{C.} \times 140$.



(a) Demagnetized



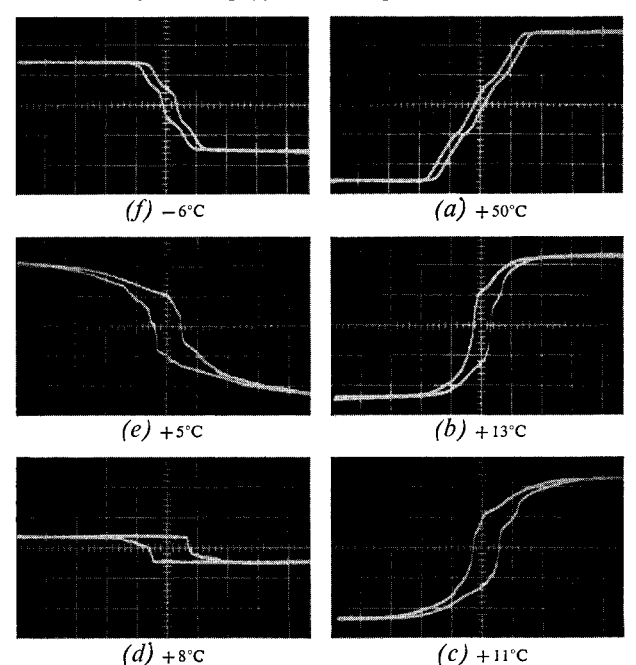
(b) In-plane field applied

On annealing, the overriding uniaxial stress anisotropy is reduced and the hysteresis loops are determined by shape and crystal anisotropy. The temperature variation of the loops for magnetization normal to the plane is shown in Fig. 8(a-f). The changing shape of the loop as a function of temperature reflects the increasing influence of shape anisotropy at temperatures removed from T_{comp} . Near T_{comp} [Fig. 8(c,e)], $M_{\rm r}/M_{\rm s}\approx 0.5$, the value expected for crystal anisotropy alone where rotation occurs to the nearest [111] directions. As the shape anisotropy increases, due to increasing magnetization, $M_{\rm r}/M_{\rm s} < 0.5$ as expected. Eventually, M_s can increase sufficiently for shape anisotropy to be dominant, and a hard-direction, nonhysteretic linear magnetization curve is approached [Fig. 8(a), T = 50 °C]. A typical room-temperature domain structure in the remanent magnetization state is shown in Fig. 9(a), where the highcontrast regions at the top and bottom are domains magnetized perpendicular to the plane of the plate and are similar to the structure in Fig. 5(a). The larger low-contrast domains in the center of the photograph are probably domains magnetized near to one of the other [111] directions at about 20° to the plane of the plate.

In contrast to the uniaxial polished (111) crystal described earlier, the in-plane hysteresis loops of the annealed (111) sample do show hysteresis; these are similar in shape to the normal loops of Fig. 8(b), where demagnetizing effects are also small.

A simple experiment was made to demonstrate the effect of strain on the total anisotropy by locally compressing the

Figure 8 *M-H* loops by Faraday effect for GdIG (111) annealed. Reduced height of loop (f) due to sample frosting.



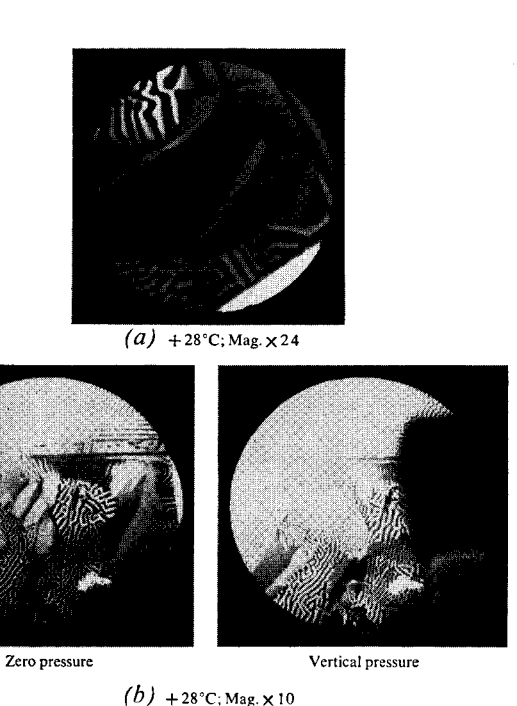


Figure 9 Domain structures on annealed GdIG (111). (a) Demagnetized. (b) Effect of vertical pressure on demagnetized structure.

sample normal to the (111). Fig. 9(b) shows that, in the vicinity of the applied pressure, the compression direction (perpendicular to the plate) becomes the preferred direction, and domains magnetized in other [111] directions change to the preferred direction. This indicates a negative magnetostriction in the [111] direction at room temperature, in agreement with Clark.⁷

• Single-crystal slab (110)

Faraday-effect hysteresis loops, at temperatures above $T_{\rm comp}$, for a polished 50- μ thick slab of GdIG (110) are shown in Fig. 10(a-f). Here the perpendicular uniaxial stress anisotropy again dominates the shape and crystal anisotropies near the compensation temperature, resulting in rectangular loops. As $M_{\rm s}$ increases at higher temperature, both curvature and shearing of the loop occurs [Fig. 10(a,b)]. The reversible curvature at high fields is due to rotation of the magnetization to the nearest [111] directions approaching the expected $M_{\rm r}/M_{\rm s}=0.82$ as shown in Fig. 10(b).

The reduced domination of the uniaxial stress anisotropy at room temperature is also exhibited by the change of loop shape with angle for the in-plane loops shown in Fig. 11(a–d). The general interpretation of these loops is that at 0° (close to an easy direction) magnetization takes place largely by domain wall motion. As the field direction is turned away from this in-plane easy direction, more of the high-field magnetization is due to rotation. In Fig. 11(d), rotation accounts for most of the magnetization.

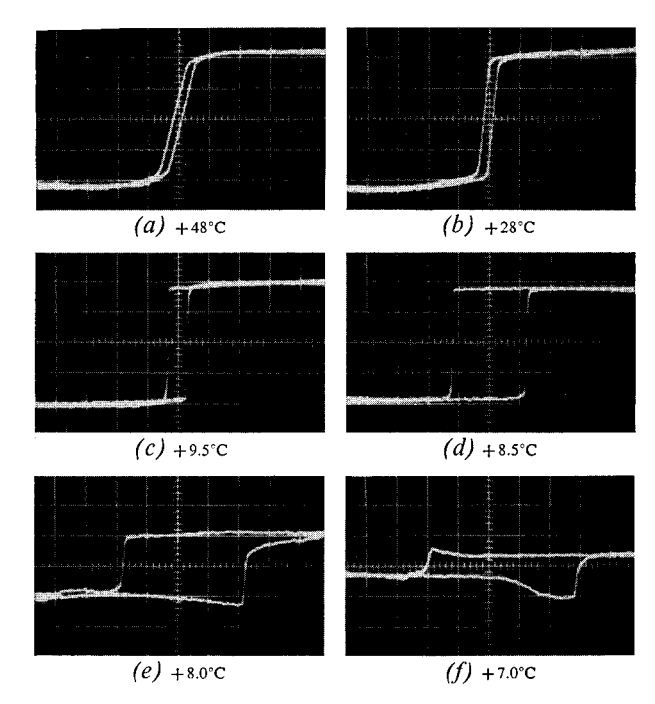
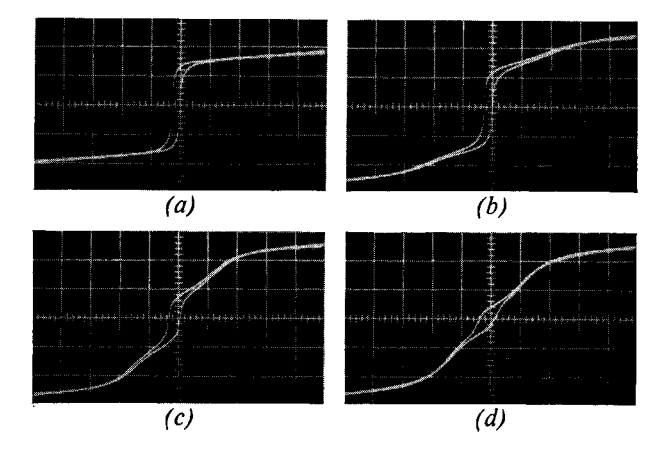


Figure 10 M-H loops by Faraday effect for GdIG (110) as polished. $H_{\text{max}} = 1850$ Oe.

Figure 11 Inductive in-plane M-H loops on GdIG (110); as polished. $H_{\rm max}=290$ Oe. $T=28^{\circ}{\rm C}$. In-plane orientation: (a) $0^{\circ}{\rm ;}$ (b) $22^{\circ}{\rm ;}$ (c) $45^{\circ}{\rm ;}$ (d) 90° . Loop height changes due to irregular sample cross section.



• Single-crystal slab (100)

For the (100) plane, no crystallographic easy directions lie either in the plane of the plate or perpendicular to it. The magnetization loops for a polished (100) slab are shown in Fig. 12(a-h). If crystal anisotropy is dominant, then rotation to the nearest easy directions would produce M_r/M_s = 0.58 after applying and removing a saturating field.

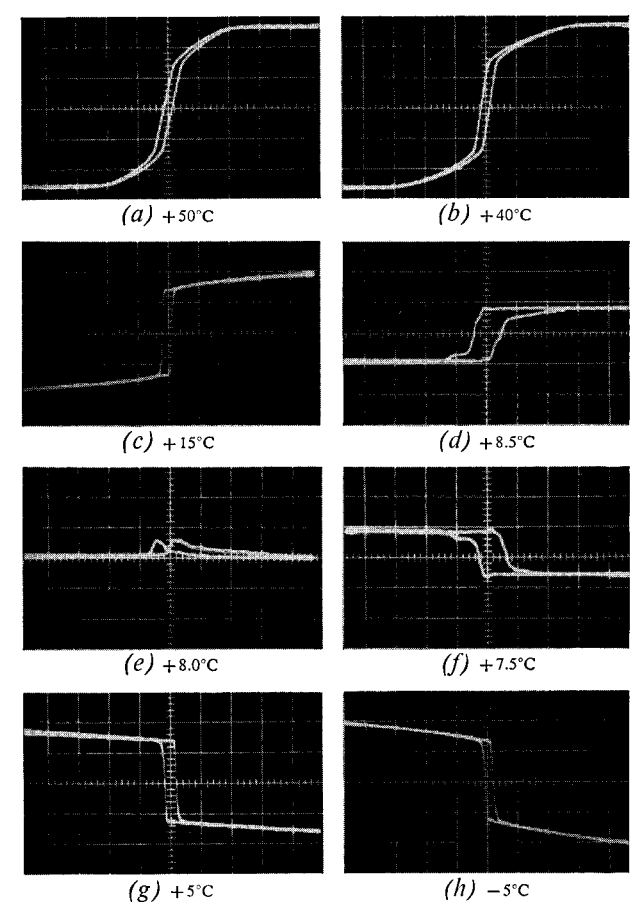


Figure 12 Faraday loops on GdIG (100) as polished. $H_{\text{max}} = 1850 \text{ Oe.}$

However, since this crystal is polished, there will again be a uniaxial stress anisotropy with its axis perpendicular to the slab plane. But, as M_s increases (greater $T-T_{comp}$), the shape anisotropy increases and opposes the stress anisotropy. At 40°C, M_r/M_s approaches 0.58 and hence the net effect of anisotropies, other than crystal anisotropy, is negligible at this temperature. Note, also, that at T = 15 °C, M_r is little changed from T = 40 °C, and so the crystal anisotropy dominates over a wide range of M_s . The room temperature in-plane loops again show some anisotropy with direction as indicated in Fig. 13(a-c). Here, the 0° and 90° directions in the plane have standard "easy direction" loops with the 45° loop showing some high-field rotation. This is again in keeping with crystal anisotropy effects since, for an in-plane field along a [100]-type direction, $M_{\rm r}/M_{\rm s}=0.82$; whereas for a [110]-directed field, $M_{\rm r}/M_{\rm s}$ = 0.58.

Also note that the in-plane coercive force is an order of magnitude less than the perpendicular H_c as measured by Faraday rotation. This would indicate that some uniaxial anisotropy is effective at room temperature.

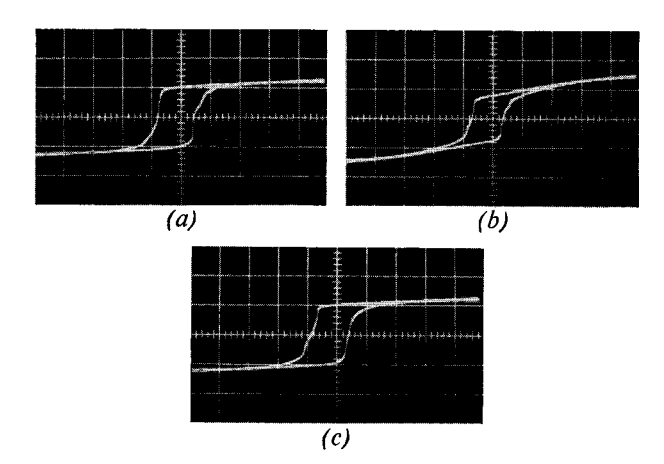


Figure 13 Inductive in-plane M-H loops on GdIG (100); as polished. (a) 0° orientation in plane; (b) 45° orientation in plane; (c) 90° orientation in plane. $H_{\text{max}} = 30$ Oe. $T = 28^{\circ}$ C.

Discussion

• (111) single crystals

At first glance, the hysteresis loops and domain structures observed in the polished (111) crystal slabs appear to be entirely analogous to the theoretical model of Kooy and Enz. Certainly, for magnetization perpendicular to the plane, the magnetization process proceeds through lateral wall motion to the formation of cylindrical domains as the applied field increases. As predicted also, this leads to a noticeable increase of the slope of the magnetization curve as $H \rightarrow H_{\text{sat}}$ (Fig. 2a).

Quantitatively, the saturation magnetization of garnets is two orders of magnitude lower than the barium ferrite studied by Kooy and Enz.⁹

The saturation magnetization for the GdIG (111) sample may be estimated from the hysteresis loops in Fig. 2 and by making use of Eq. 1. Near the compensation temperature [e.g., Fig. 2(c,d,e)], $H_1 > 4\pi M_s$; hence the nucleation field H_n falls rapidly for small temperature changes from T_{comp} . However, at high temperatures H_n changes less with temperature increase and is estimated to be about 25 Oe in the temperature range of 25 to 30°C. Thus, at 25°C, using Eq. (1), $M_s \approx 3.8$ gauss. This estimate is in good agreement with a direct measurement of M_s made at 25°C.

We may now roughly estimate the effective uniaxial anisotropy, due to strain and crystal anisotropy, from the field required to produce saturation in the "hard" direction; that is, from the "in plane" magnetization curve Fig. 6(a-d). These loops are nonhysteretic and isotropic in the plane, as would be expected for a dominating uniaxial anisotropy. The nonconstant slope is, however, a departure from the simple uniaxial model, and a purely rotational process is assumed only for small fields. Assuming then that the

saturation field, H_s , is that required to turn the magnetization through 90° against the induced uniaxial anisotropy (but aided by the shape anisotropy),

$$H_{\rm s} = 2K_{\rm u}/M_{\rm s} - 4\pi M_{\rm s} \,, \tag{3}$$

where $K_{\rm u}$ is the induced uniaxial anisotropy. From Fig. 6(a), $H_{\rm s}=700$ Oe, and, as estimated, $M_{\rm s}=3.8$ gauss at 25°C, and

$$K_{\rm u} = 0.5 M_{\rm s} (H_{\rm s} + 4\pi M_{\rm s}) \quad 1.4 \times 10^3 \,{\rm erg/cm}^2$$

which is of similar magnitude to the measured crystal anisotropy at room temperature in single-crystal GdIG. ¹⁰ However, the above estimation of $K_{\rm u}$ may be somewhat low due to the assumption of a truly rotational process at low fields.

We may now proceed to apply the analysis of Kooy and Enz to estimate the domain wall energy in the (111) GdIG. The total energy of the simple line domain structure shown in Fig. 14 is made up of wall energy $E_{\rm w}$, energy of the magnetization in the applied field $E_{\rm h}$, and self-demagnetization energy $E_{\rm d}$. On equating to zero the derivatives of the total energy $E = E_{\rm w} + E_{\rm d} + E_{\rm h}$ with respect to the domain size, the magnetization curve can be calculated for various sample thicknesses⁹ as shown in Fig. 15. Here, saturation is reached for $H < 4\pi M_s$ for thin samples. The predicted curvature is observed in the experimental hysteresis loops of Fig. 2. Also, in practice, we observe that the simple line domain structure reduces to small circles as $H \rightarrow H_s$ and that these have constant diameters before disappearing at $H = H_{\rm s}$. Kooy and Enz calculated this critical radius to be given by

$$R_c = (\sigma_{\rm w} D [1 + \mu^{\frac{1}{2}}])^{\frac{1}{2}} / 8 M_{\rm s}, \tag{4}$$

where $\sigma_{\rm w}=$ specific wall energy, and $\mu=1+2\pi M_{\rm s}^2/\ K_1\approx 1$ for garnets.

From the observed domain structure, $R_{\rm e} \approx 8\mu$ at 25°C. Also, $M_{\rm s} = 3.8$ gauss and $D = 58\mu$. Hence, $\sigma_{\rm w} = 0.1$ erg/cm².

We are now able to estimate the thickness of the 180° Bloch walls in the garnet crystals. For a crystal with uniaxial anisotropy, the wall thickness δ is given by¹¹

$$\delta = \pi (A/K_{\rm u})^{\frac{1}{2}},\tag{5}$$

where K_u is the uniaxial anisotropy, and A is the exchange constant. Further, the wall energy is given by¹¹

$$\sigma_{\mathbf{w}} = 4(AK_{\mathbf{u}})^{\frac{1}{2}}. \tag{6}$$

Hence

$$\delta = \pi \sigma_{\rm w/4K_{\rm u}} \tag{7}$$

Substituting in Eqs. (6) and (7), we obtain $A=45 \times 10^{-8}$ erg/cm and $\delta=0.6$ microns.

The width of the walls can be roughly estimated from domain patterns such as Fig. 7(a), since the analyzer and

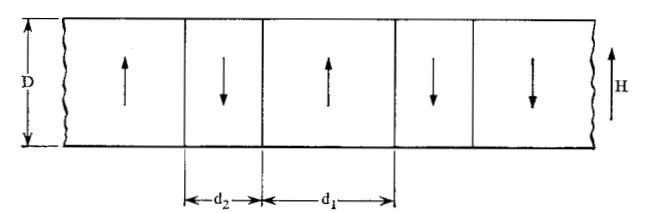
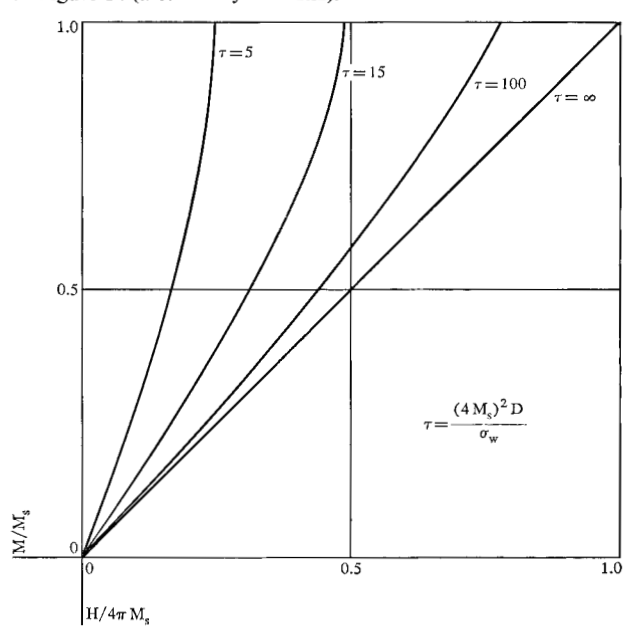


Figure 14 Simple 180° domain structure for applied field H perpendicular to plate of thickness D_{\bullet}

Figure 15 Theoretical magnetization curves for domain structure of Figure 14 (after Kooy and Enz).



polarizer are adjusted to produce less transmission for the magnetization in the wall than in the neighboring domains. From these pictures, a wall width \sim 2 microns is estimated. However, due to nonstraightness of walls through the sample thickness, we expect this estimate to exceed the actual wall thickness. The value for the exchange constant is similar to measured values for YIG determined in a variety of ways. 12

Summarizing, the theoretical analysis of Kooy and Enz for the magnetization curve of a simple uniaxial material, with 180° Bloch walls, along the easy axis seems to be applicable to the magnetization curves and domain structures observed in a (111) GdIG plate with a stress-induced easy axis perpendicular to its plane. An estimate of a uniaxial anisotropy of $K_{\rm u}=1.4\times10^3\,{\rm erg/cm^3}$, a wall energy $\sigma_{\rm w}=0.1\,{\rm erg/cm^2}$ and a wall thickness $\delta=0.6$ microns and an exchange constant of $A=45\times10^{-8}\,{\rm erg/cm}$ is obtained from the experimental results.

Acknowledgments

The single-crystal garnet slabs were kindly supplied by E. A. Giess. The Faraday-effect hysteresigraph was designed and constructed by J. W. Beck, R. E. MacDonald, and D. Murphy. The high quality of the domain photographs is due to the skill of E. B. Moore. Similar *M-H* loops to those shown in Fig. 2 were observed by J. Greiner, IBM Watson Research Center, Yorktown, using a d-c Faraday-effect hysteresigraph. The direct magnetization measurements were made by H. Lillienthal using a force balance magnetometer.

References

- J. T. Chang, J. F. Dillon, U. F. Gianola, J. Appl. Phys. 36, 1110 (1965).
- 2. C. D. Mee and G. Fan, *IEEE Trans. Magnetics*, 3, No. 1, 72-6 (1967).
- 3. J. F. Dillon and H. E. Earl, Amer. J. of Phys. 27, 201 (1959).

- 4. J. W. Beck, to be published in Rev. Sci. Instr.
- J. Miyata and T. Lentz, Large Capacity Memories Conference Report, Macmillan, 1962, pp. 117–134.
- C. D. Mee, Physics of Magnetic Recording, Wiley, 1964, p. 221.
- A. E. Clark, B. F. DeSavage, E. R. Callen, J. Appl. Phys. 35, Part 2, 1028 (1964).
- 8. B. Luthi and T. Henningsen, *Proceedings of International Conference in Magnetism*, Nottingham; Inst. of Physics, 1964, p. 668.
- 9. C. Kooy and U. Enz, Philips Res., Reports 15, 7-29 (1960).
- B. A. Calhoun, W. V. Smith, J. Overmeyer, J. Appl. Phys. 29, 427 (1958).
- 11. S. Chikazumi, *Physics of Magnetism*, John Wiley, 1964, p. 191
- 12. E. E. Anderson, Phys. Rev. 134A, 1581 (1964).

Received October 24, 1966.